PHYSICAL REVIEW B **66**, 060102(R) (2002)

Viscosity of liquid Fe at high pressure

Michael D. Rutter, Richard A. Secco, and Hongjian Liu
Department of Earth Sciences, University of Western Ontario, London, Ontario, Canada N6A 5B7

Takeyuki Uchida, Mark L. Rivers, Stephen R. Sutton, and Yanbin Wang
Consortium for Advanced Radiation Sources, University of Chicago, 5640 S. Ellis Ave., Chicago, Illinois 60637

(Received 15 May 2002; published 14 August 2002)

Synchrotron x-ray radiography has been used to measure the viscosity of pure liquid Fe at high pressure and temperature in a large volume press. A probe sphere rising through liquid Fe at high pressure and temperature is imaged, *in situ*, allowing for the derivation of sample viscosity through a modified form of Stokes' equation. The effect of pressure on viscosity is fit by the semi empirical framework for transport coefficients in liquid metals, providing experimental verification of constant viscosity at the pressure-dependent melting temperature of liquid Fe where no change in liquid structure occurs.

DOI: 10.1103/PhysRevB.66.060102 PACS number(s): 66.20.+d, 61.25.Mv, 62.50.+p

The physical properties of Fe, both liquid and solid, have long been the backbone upon which our understanding of the formation, differentiation, structure, and dynamics of planetary bodies has been based. Specifically, the viscosity of liquid Fe is an essential parameter to model and understand fundamental core processes such as the generation of the Earth's magnetic field. The importance and relatively unknown nature of the effect of pressure on liquid Fe viscosity, to both the geophysical and the broad materials science communities, has sparked many studies to elucidate this question. Initial measurements on the high-pressure viscosity of an Fe-FeS alloy suggested that the physics of Fe alloy systems under pressure is much more complicated than suggested by theory.[1] Following these initial measurements, considerable efforts have been invested in determining the dynamic properties of liquid Fe and Fe alloys under high pressure, through both computational (*ab initio*, molecular dynamics),[2–6] and experimental[7,8] techniques. However, there is still an absence of sound experimental data quantifying the effect of pressure on the viscosity of pure liquid Fe. This is largely due to the extreme experimental conditions that must be maintained and controlled in order to measure the dynamic fluid properties of liquid Fe under pressure. Very recently, through the development of a new technique, we have measured the effect of pressure on an Fe alloy with low S content (8.5-wt. % S) and find constant viscosity behavior at the melting temperature.[9] This provided an experimental verification that the effect of pressure on the viscosity of Fe-FeS alloys can be quantified through its effect on the pressure-dependent melting boundary. Therefore, in order to understand the complex behavior of Fe and Fe alloys under pressure, a detailed study of the pure liquid Fe end member is required. Here we present measurements of the viscosity of pure liquid Fe at pressures up to 5.5 GPa and isothermally at 2050 K using synchrotron x-ray radiography, demonstrating a constant viscosity along the pressure-dependent melting boundary within a single liquid (i.e., constant melt structure) phase.

High pressure and temperature experiments were carried out in a 250 ton, DIA-type, large volume press (LVP) on the GSECARS 13-BMD beamline[10] at the Advanced Photon Source. X-ray radiography was used to image *in situ* a probe sphere rising through the liquid Fe sample at high pressure. Using a modified form of Stokes' law, the sample viscosity can be determined from the terminal velocity of the probe sphere. The x-ray radiographic technique images the pressurized region within the LVP according to the relative X-ray attenuation coefficients of the experimental materials.[11] Consequently, to image a probe sphere requires it to have a greater x-ray attenuation coefficient and a higher melting temperature than the surrounding liquid Fe sample. Unfortunately, most materials which fit these criteria also have an affinity for reacting with liquid Fe. Therefore, to eliminate any reaction between the x-ray visible portion of the probe sphere, which we chose as Pt, a technique was developed to encapsulate the Pt core in a ruby mantle to produce a composite sphere.[12] All radiographic experiments were carried out using incident x-rays in the energy range 20–120 keV.

Solid Fe samples (99.9% purity) were machined to a cylinder 2.5 mm high and 1.5 mm in diameter and contained in a hexagonal boron nitride (hBN) sample container. A small pit was drilled in the base of the Fe sample to accept the probe sphere. Pressure was determined using the known equation of state of MgO (Ref. 13) and by measuring the lattice constants of an MgO pressure marker, which replaced the upper lid of the hBN cup. High temperature was generated by resistance heating of a cylindrical graphite furnace and temperature was monitored by a WRe(3%)-WRe(25%) thermocouple. No pressure correction was applied to the measured temperatures, and gradients within the sample were estimated at ± 50 K. During each experiment, the pressure temperature path was as follows: (i) pressure was increased to the target at ambient temperature, (ii) temperature was ramped to ~ 500 K below the run temperature where the sample equilibrated in the solid state; and (iii) temperature was abruptly increased to the experimental temperature where the sample melted and the probe sphere rose.

Radiographic images of the vertical flight of the probe sphere were collected on standard VHS videotape at 30 frames per second, and subsequently digitized. A series of images of the ascent of the probe sphere through the liquid Fe sample is illustrated in Fig. 1(a). The Pt core of the

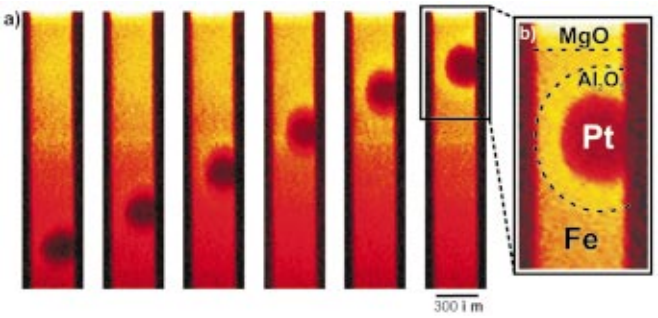

FIG. 1. (Color) (a) X-ray radiographic sequence of images of the vertical flight of a probe sphere through liquid Fe at 2050 K and 4.5 GPa. The time between frames is ~70 msec, and the Pt core is seen as the dark circular region which rises as the frames advance. (b) Enhanced view of a probe sphere in liquid Fe near the MgO lid of the sample container. The dark bars which bracket the sample are the tungsten carbide anvils of the press.

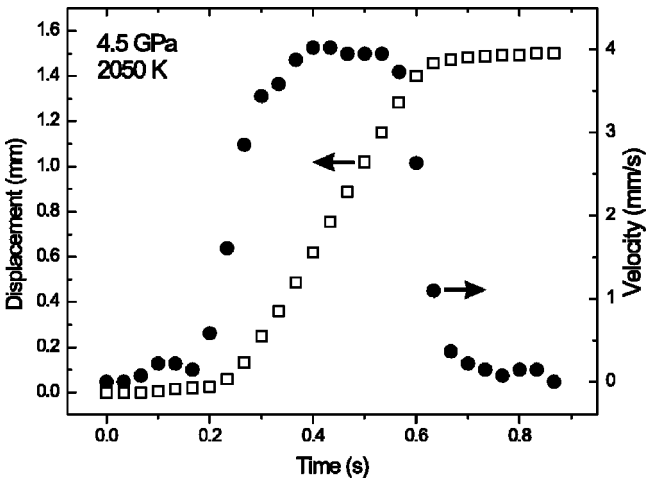

FIG. 2. Displacement and velocity vs time curves for the flight of the probe sphere in liquid Fe at 4.5 GPa and 2050 K.

probe sphere is clearly seen as the dark circular region rising the length of the liquid sample as the frames advance. The total elapsed time during the vertical flight of the probe sphere is <1 sec. The dark bars which bracket the sample are the tungsten carbide anvils of the press. Due to their high x-ray attenuation they are opaque and restrict x-ray access to the central third of the high pressure environment. Figure 1(b) illustrates the key visible experimental components at the end of the probe sphere's flight. The continuity of the probe sphere is clearly seen, suggesting that any reaction between the Fe liquid and the Pt sphere has been eliminated. Sectioning of the recovered samples and electron-probe microanalysis examination confirmed that no reaction occurred between the Fe sample, the probe sphere, and the sample container. Additionally, the vertical motion of the sphere, which would not occur if residual solid portions of the sample were present, attests to the homogeneous, entirely liquid phase present.

From the radiographic images of the sphere's ascent through the liquid sample, the velocity of the sphere can be extracted. The displacement and velocity *vs*. time for the probe sphere's flight is given in Fig. 2. To successfully measure the viscosity of the liquid Fe sample, it is necessary that the velocity of the probe sphere be terminal (i.e., constant velocity *vs* time). The sigmoidal nature of the displacement curve is indicative of the acceleration of the probe sphere, as it is released from the base of the sample after the Fe sample has melted, the terminal velocity of the sphere during the bulk of its passage through the melt, and the deceleration as it approaches the container lid. The terminal velocity of the sphere is further reinforced in the large plateau of the velocity curve.

The corrected form of Stokes' equation used to determine the viscosity of the sample is as follows:

$$\eta = \frac{2gr_s^2(\Delta\rho)}{9\nu}\frac{W}{E}, \tag{1}$$

where η is the sample dynamic viscosity, g is gravitational acceleration, r_s is the radius of the probe sphere, $\Delta\rho$ is the density contrast between the sphere and the liquid, ν is the terminal velocity of the sphere and W and E are empirical corrections for the effects of the finite wall and ends of the sample container, respectively $(W/E \sim 0.2)$.[14,15] From Eq. (1), it is evident that in addition to making an accurate measurement of the terminal velocity of the probe sphere to determine sample viscosity, the relative densities of the sphere and the liquid Fe sample must be known. To accurately determine the density of the probe sphere, measurements of the volumes of the Pt and ruby components of the sphere were made at ambient conditions on the quenched samples by x-ray computed microtomography (CMT).[16] For CMT analysis, the recovered and unperturbed Fe sample, containing the probe sphere, was placed on a rotation stage in a monochromatic x-ray beam with an energy of 45 keV. The x rays penetrated the sample as it was rotated through 180° in 0.5° increments, allowing for the rendering of a digital three-dimensional image of the sample with a resolution of $<4\mu m$. This image was then virtually sliced along each plane at successive depth intervals and the areas of the Pt and ruby components were measured. Figure 3 illustrates an example of a CMT image sliced perpendicular [Fig. 3(a)] and parallel to [Fig. 3(b)] the long axis of the cylindrical Fe sample. The Pt core of the probe sphere appears as the white circular region while the ruby mantle is the dark rim bracketing the Pt core from the Fe sample (gray). The continuity of the ruby mantle can be verified in three dimensions, confirming it acts as a successful barrier between the Pt core and the liquid Fe. Plotted in Fig. 3(c) are the measured areas of the Pt core and ruby mantle as the sample was sliced. The density of the probe sphere at the experimental pressure and temperature was calculated with the high-temperature third order Birch-Murnaghan equation of state and the thermoelastic parameters for Pt and ruby[17–19]

Measured terminal velocity and density of the probe sphere and the calculated melt density and sample viscosity are given in Table I. Viscosity data, derived from individual experiments at 2050 K, are plotted as a function of pressure in Fig. 4 (solid diamonds).

Upon first inspection of the data, the effect of pressure on

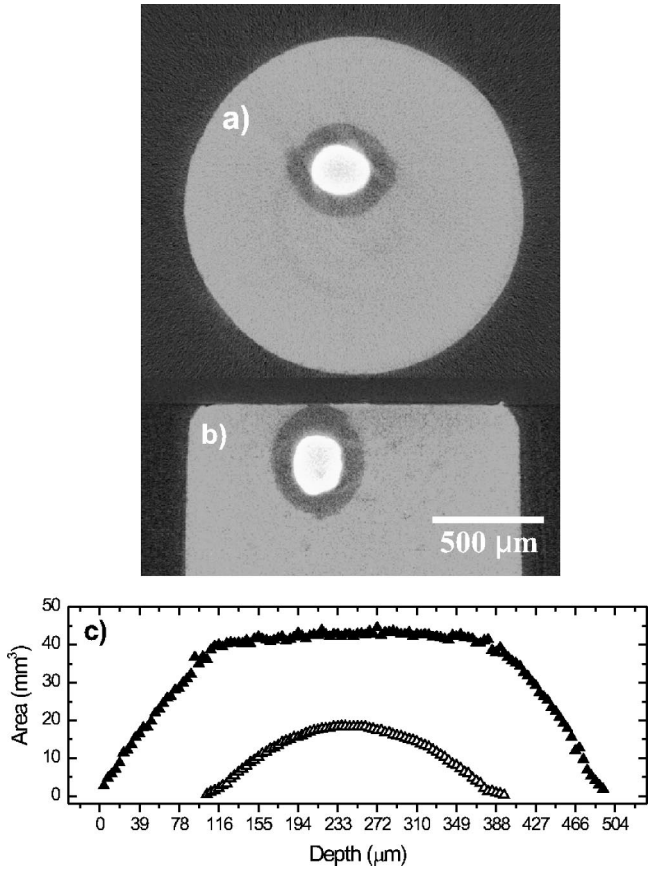

FIG. 3. X-ray computed microtomographic (CMT) image of the unperturbed Fe sample and probe sphere post-experiment, virtually sliced perpendicular to (a) and parallel to (b) the long axis of the cylindrical sample. (c) Measured area of the ruby mantle (solid triangles) and the Pt core (open triangles) at successive slices of the CMT image through the probe sphere.

the viscosity of liquid Fe is small and the data agree well with the room pressure experimental (solid circle) (Ref. 21) and theoretical (open circle) (Ref. 22) values. This result contrasts sharply with our recent measurements of a liquid Fe-FeS alloy (8.5-wt.% S) which indicate a large effect of pressure on viscosity.[9] The semi-empirical theory[23] describing transport properties in liquid metals under pressure, which until now has not been confirmed in pure liquid Fe, is

TABLE I. Measured probe sphere density, terminal velocity, calculated melt density, and sample viscosity.

Pressure (GPa)	Probe sphere density[a] (g/cm^3)	Terminal velocity (mm/s)	Melt density[b] (g/cm^3)	Sample Viscosity (mPa s)
1.6	6.78±0.20	2.6±0.1	7.00	2.36
4.5	6.62±0.20	4.0±0.1	7.26	4.80
5.5	6.84±0.21	4.3±0.5	7.35	3.56

[a]measured by x-ray computed microtomography of recovered samples.
[b]Reference 20.

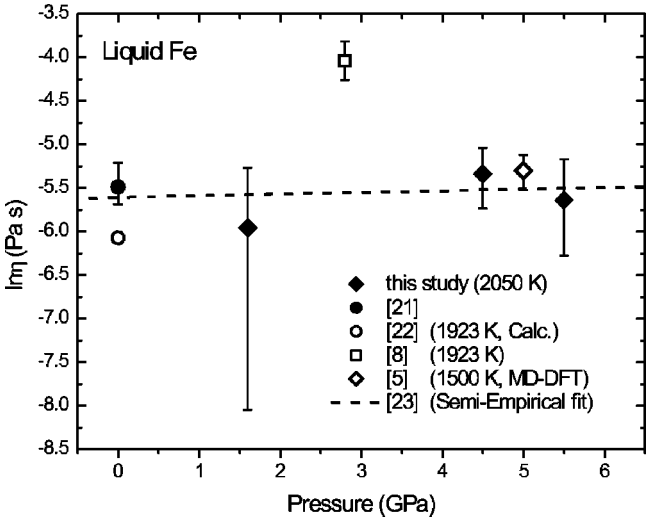

FIG. 4. Effect of pressure on the viscosity of liquid Fe at 2050 K. Solid diamonds are the data points measured in this study, the solid circle is the room pressure value taken from Ref. 21, the open circle is the first principles and molecular dynamics computation value of Ref. 5, the open square is the experimentally measured value of Ref. 8, and the dashed line is the semi-empirical fit from Ref. 23. Large error bars on the 1.6 GPa data point are due the error in $\Delta\rho$ which dominates Eq. (1)

used to fit our data. It has been demonstrated both empirically and theoretically that for liquid metals the following relation holds:[23]

$$\Delta V_\eta^* = 0.04 V_{atomic}, \tag{2}$$

where V_{atomic} is the atomic volume of the liquid, and ΔV_η^* is the apparent activation volume of viscosity which quantifies the effect of pressure on viscosity through an Arrhenian dependence as follows:

$$\Delta V_\eta^* = RT\left(\frac{\partial \ln \eta}{\partial P}\right)_T \tag{3}$$

Moreover, from Eq. (2) it has been demonstrated that, for liquid metals, viscosity is constant along the melting boundary. Assuming that no change in liquid structure occurs in the pressure and temperature region examined, the effect of pressure on viscosity can be quantified through its corresponding effect on the melting curve. Changes in the liquid structure of Fe at high pressure have been proposed as the source of marked changes in other physical property behavior, viz electrical resistivity.[24] X-ray-diffraction measurements on liquid Fe (Ref. 25) have shown that in the vicinity of the Fe $\delta-\gamma-l$ triple point liquid Fe undergoes changes in short-range ordering (bcc to bcc+fcc structure) with increasing pressure and temperature. However, the temperature condition at which the onset of this transition occurs is ~200 K above the temperature at which the present experiments were carried out. Therefore, there is no evidence of any change in short range liquid structure within the pressure and temperature conditions explored in this study. Taking the apparent activation volume as 4% of the atomic volume, the predicted

effect of pressure on viscosity is shown in Fig. 4 by a dashed line. The theoretical line successfully fits our data and the room pressure data well. The theoretical fit to our data implies that the viscosity of liquid Fe can be scaled to its melting boundary allowing for the determination of viscosity in the pressure range for which the melting curve of Fe is known. Additionally, the viscosity value determined for Fe in Ref. 5 through a first-principles, molecular-dynamics study, coincides with our experimental data at similar pressures and falls on the theoretical fit to the data (Fig. 4). The high-pressure viscosity datum determined in Ref. 8, which is plotted in Fig. 4, falls outside the viscosity region defined by our experiments and theory. Given the apparent activation energy of viscosity ($\sim$40 kJ/mol) for liquid Fe at room pressure[26] a correction for the effect of temperature on viscosity to 2050 K is insufficient to bring it in line with our data. Most likely, reactions in their sample environment and limited visual resolution are the sources of the discrepancy.

The importance of the experimental measurements of the viscosity of pure liquid Fe under high pressure is twofold. First, these data show the effect of pressure on liquid Fe viscosity, which can be used to address the nature and behavior of dynamic liquid properties in liquid Fe and Fe alloys at high pressure. Second, the agreement between the semi-empirical theory and the experimental values confirm constant viscosity at the pressure dependent melting boundary for pure liquid Fe. This portends well for prediction of viscosity along the high pressure melting boundary on the basis of the more easily determined 1 atm value of other liquid metals that do not undergo changes in liquid structure.

R.A.S. acknowledges support from a Natural Sciences and Engineering Research Council of Canada grant. Radiography experiments were carried out at GeoSoilEnviroCARS (GSECARS), Sector 13, Advanced Photon Source at Argonne National Laboratory. GSECARS is supported by the National Science Foundation-Earth Sciences, Department of Energy-Geosciences, W. M. Keck Foundation and the United States Department of Agriculture. Use of the Advanced Photon Source was supported by the U.S. Department of Energy, Basic Energy Sciences, Office of Science, under Contract No. W-31-109-Eng-38. We thank R. Tucker for the preparation of composite spheres and experimental cell components.

[1] G.E. Leblanc and R.A. Secco, Geophys. Res. Lett. **23**, 213 (1996).

[2] L. Vočadlo, G.A. de Wijs, G. Kresse, M. Gillan, and G.D. Price, Faraday Discuss. **106**, 205 (1997).

[3] G.A. de Wijs, G. Kresse, L. Vočadlo, D. Dobson, D. Alfé, M.J. Gillan, and G.D. Price, Nature (London) **392**, 805 (1998).

[4] D. Alfé, G. Kresse, and M.J. Gillan, Phys. Rev. B **61**, 132 (2000).

[5] L. Vočadlo, D. Alfé, G.D. Price, and M.J. Gillan, Phys. Earth Planet. Inter. **120**, 145 (2000).

[6] Y. Zhang, G. Guo, and G. Nie, Phys. Chem. Miner. **27**, 1640 (2000).

[7] D.P. Dobson, W.A. Crichton, L. Vočadlo, A.P. Jones, Y. Wang, T. Uchida, M. Rivers, S. Sutton, and J.P. Brodholt, Am. Mineral. **85**, 1838 (2000).

[8] H. Terasaki, T. Kato, S. Urakawa, K. Funakoshi, A. Suzuki, T. Okada, M. Maeda, J. Sato, T. Kubo, and S. Kasai, Earth Planet. Sci. Lett. **190**, 93 (2001).

[9] M.D. Rutter, R.A. Secco, T. Uchida, H. Liu, Y. Wang, M.L. Rivers, and S.R. Sutton, Geophys. Res. Lett. **29**, 58-1 (2001).

[10] M.L. Rivers, T.S. Duffy, Y. Wang, P.J. Eng, S.R. Sutton, and G. Shen, in *Properties of the Earth and Planetary Materials at High Pressure and Temperature*, edited by M.H. Manghnani and T. Yagi (American Geophysical Union, Washington, DC, 1998), p. 79.

[11] M. Kanzaki, K. Kurita, T. Fujii, T. Kato, O. Shimomura, and S. Akimoto, in *High-Pressure Research in Mineral Physics*, edited by M. H. Manghnani and Y. Syono ((American Geophysical Union, Washington, DC, 1987), p. 195.

[12] R.A. Secco, R.F. Tucker, P.S. Balog, and M.D. Rutter, Rev. Sci. Instrum. **72**, 2114 (2001).

[13] W. Utsumi, D.J. Weidner, and R.C. Liebermann, in *Properties of the Earth and Planetary Materials at High Pressure and Temperature* (Ref. 10), p. 327.

[14] H. Faxen, Ark. Mat. Astron. Fys. **19**, 1 (1925).

[15] W. D. Kingery, *Property Measurements at High Temperature* (John Wiley and Sons, New York, 1959).

[16] M.L. Rivers, S.R. Sutton, and P. Eng, Proc. SPIE **3772**, 78 (1999).

[17] N.C. Holmes, J.A. Moriarty, G.R. Gathers, and W.J. Nellis, J. Appl. Phys. **66**, 2962 (1989).

[18] O.L. Anderson and D.G. Isaak, in *Mineral Physics and Crystallography: A Handbook of Physical Constants*, edited by T.J. Ahrens (American Geophysical Union, Washington, DC, 1995), p. 64.

[19] Y. Fei, in *Mineral Physics and Crystallography: A Handbook of Physical Constants* (Ref. 18), p. 29.

[20] P.M. Nasch and M.H. Manghnani, in *Properties of the Earth and Planetary Materials at High Pressure and Temperature* (Ref. 10), p. 307.

[21] R.A. Secco, in *Mineral Physics and Crystallography: A Handbook of Physical Constants* (Ref. 18), p. 218.

[22] I. Yokoyama and T. Arai, J. Non-Cryst. Solids **293-295**, 806 (2001).

[23] J.P. Poirier, Geophys. J. **92**, 99 (1988).

[24] R.A. Secco and H.H. Schloessin, J. Geophys. Res. **94(B5)**, 5887 (1989).

[25] C. Sanloup, F. Guyot, P. Gillet, G. Fiquet, R.J. Hemley, M. Mezouar, and I. Martinez, Europhys. Lett. **52**, 151 (2000).

[26] J.P. Poirier, *Introduction to the Physics of the Earth's Interior* (Cambridge University Press, Cambridge, 2000).